l

Southern Ocean control of near-future global warming rates in climate models

So-Jung Shin[1], Sang-Wook Yeh[2]*, Soon-Il An[1,3]*, Noel Keenlyside[4], Shang-Ping Xie[5], and

Jae-Heung Park[3]

[1] Department of Atmospheric Sciences and Irreversible Climate Change Research Center, Yonsei University, Seoul 03722, Korea

[2] Department of Marine Science and Convergence Engineering, Hanyang University, ERICA, Ansan 15588, Korea

[3] Division of Environmental Science and Engineering, Pohang University of Science and Technology, Pohang 37673, Korea

[4] Geophysical Institute, University of Bergen and Bjerknes Centre for Climate Research, Bergen, Norway

[5] Scripps Institution of Oceanography, University of California San Diego, La Jolla CA 92093, USA

*Corresponding author:

Prof. Soon-Il An, Department of Atmospheric Sciences, Yonsei University, Seoul, 03722, South Korea (sian@yonsei.ac.kr)

*2nd Corresponding author:

Prof. Sang-Wook Yeh, Department of Marine Science and Convergent Engineering, Hanyang University, ERICA, Ansan, South Korea (swyeh@hanyang.ac.kr)

Key Points:

- Inter-model diversity of the Paris Agreement targets of 1.5C°/2°C warming is considerable in CMIP type climate models.
- A 2°C near-future global warming rate is determined by Southern Ocean state closely tied with a low-level cloud amount feedback strength during the reference period.
- Climate models with cold Southern Ocean tend to accompany more low-level cloudiness and Antarctic SIC due to a strong low-level cloud amount feedback.

Abstract

Global warming will soon reach the Paris Agreement targets of 1.5C°/2°C temperature increase. Under a business-as-usual scenario, the time to reach these targets varies widely among climate models. Using Coupled Model Intercomparison Project phase 5 and 6, we show that a 2°C near-future global warming

rate is determined by Southern Ocean (SO) state closely tied with a low-level cloud (LLC) amount feedback strength during the reference (1861-1900) period; climate models with cold SO tend to accompany more low-level cloudiness and Antarctic sea ice concentration due to a strong LLC amount feedback. Consequently, initially cold SO models tend to simulate a fast near-future warming rate by absorbing more downward shortwave radiation compared to initially warm SO models because more LLC disappears due to a strong LLC amount feedback during the 2°C rise. Our results demonstrate that climate models that correctly simulate initial SO state can improve near-future projections with reduced uncertainties.

Plain Language Summary

In December 2015 at Paris, United Nations agreed to hold the increase in the global average temperature to "well below" 2{degree sign}C above pre-industrial levels and pursuing efforts to limit 1.5{degree sign}C above pre-industrial levels. It naturally leads to a question as to when these targets will reach. However, under a business-as-usual scenario, the time to reach these targets varies widely among climate models. Using Coupled Model Intercomparison Project phase 5 and 6, we show that a 2{degree sign}C near-term global warming rate is closely related to the late 19th century condition of Southern Ocean (SO) state such that the initially cold SO climate models actually produced fast near-term warming rate and vice versa. This is because these initially cold SO climate models that mostly accompany more low-level cloudiness and Antarctic sea ice concentration, could actually absorb more downward shortwave radiation by reducing cloudiness and sea-ice during a warming progress compared to initially warm SO models. Finally, our results demonstrate that climate models that correctly simulate initial SO state can improve near-term projections with reduced uncertainties.

1. Introduction

Various feedback processes can accelerate (or slow down) global mean surface temperature (GMST) warming induced by greenhouse gas concentration increase (Scheffer et al., 2006). Observational records show a GMST warming rate of about 0.068°C/decade since 1880, although natural variability on the low-frequency timescales may cause large fluctuations (Figure 1a). Despite international efforts to suppress GMST increase (Masson-Delmotte et al., 2018), temperatures have risen almost 1.1°C over 1850 to 2019 (Masson-Delmotte et al., 2021). After a slow rise at the beginning of the 21st century, rapid increase in GMST, accompanied by extreme weather and climate events such as heatwaves and droughts, is observed (e.g., Briffa et al., 2009; Christidis et al., 2011; Dai, 2011; Duffy & Tebaldi, 2012).

In December 2015, the Paris Agreement adopted a 1.5°C/2°C overall GMST increase limit. Since then, many studies have tried to understand how a 1.5°C/2°C warming might influence human well-being, sea ice cover, sea level height, biodiversity, extreme natural events, and hydrological cycles (e.g., Donnelly et al.,

2017; Baker et al., 2018; Brown et al., 2018; Ebi et al., 2018; Niederdrenk & Notz, 2018; Smith et al., 2018). Despite this wealth of studies, there is little understanding of the physical factors modulating the near-future global warming rates. The Coupled Model Intercomparison Project Phase 5 and Phase 6 (CMIP5/CMIP6) climate models show a wide variety of simulation outcomes along with large uncertainties (Figure 1b and Figure S1a). Understanding what physical factors modulate near-future warming rates is critical because mitigating and adapting to climate change impacts are considerably time-sensitive.

In general, climate model warming rates are determined by the model's climate sensitivity and constrained by physical processes including i) radiative forcing (Knutti et al., 2017), ii) cloud feedback (Cess, 1990; Bony & Dufresne, 2005; Soden & Held, 2006; Zelinka et al., 2020), and iii) ocean heat uptake (Raper et al., 2002; Winton et al., 2010; Geoffroy et al., 2013; Frölicher et al., 2014). There are fewer studies, however, of how the climate state in the reference period produced by climate models might affect near-future warming rates of 1.5°C/2°C in future climate scenarios (Dommenget, 2016; Kajtar et al., 2021). In this study, we suggest a new perspective on model-predicted near-future global warming rates of 1.5°C/2°C in CMIP5/CMIP6 climate models- that they are determined by the Southern Ocean (SO) surface temperature state along with a strength of low-level cloud (LLC) amount feedback during the reference period. Understanding these processes will help improve near-future projections with reduced uncertainty. We chose Representative Concentration Pathway (RCP) 8.5 and Shared Socioeconomic Pathway (SSP) 5-8.5 scenarios, i.e., business-as-usual scenarios to highlight the case of no mitigation and to focus on greenhouse gas-induced warming through the model's response to strong radiative forcing. In spite of this, it is noteworthy that the multi-model ensemble means of timings for near-future warming (1.5^{o}~2^{o}C) in RCP2.6 and SSP1-2.6, the scenarios compatible with the 2^{o}C target, are not very different from those in RCP8.5 and SSP5-8.5. In this paper, CMIP5 results will be mainly presented and CMIP6 results discussed further later.

2. Data and Methods

2.1 GMST observation and CMIP5/CMIP6

We used observed annual GMST time series data for 1861–2019 from the Met Office Hadley Centre observations datasets (HadCRUT4) (Morice et al., 2012). The raw time series data presented as temperature anomalies relative to 1961-1990 were converted to anomalies compared to 1861-1900, defined as the reference period in this study.

We used monthly output data of historical and RCP8.5 simulations for the Coupled Model Intercomparison Project phase 5 (CMIP5) and historical and SSP5-8.5. simulations for CMIP6, respectively. Only the first ensemble member (i.e., r1i1p1 for CMIP5 and r1i1p1f1 for CMIP6) was chosen. We used 37 CMIP5 and 26 CMIP6 climate models to examine the diversity of warming rates to 1.5°C/2°C warming targets between climate models. However, there is a limit

to the available models for the variables required for analysis, so only some of 37 CMIP5 or 26 CMIP6 climate models are used for some analyses.

2.2 Near-future global warming timing and rate to 1.5°C/2°C rise

The reference period was 1861-1900 in the historical simulation, following the pre-industrial period used in the AR5 and IPCC special report and taking into account the different initial integration times of the historical experiments from model to model. Using the surface air temperature data, the annual mean GMST time series was obtained and smoothed by an 11-year moving average for each model. Based on the smoothed GMST time series, the 1.5°C (2°C) increase period was defined as years under historical and RCP8.5 (or SSP5-8.5) scenarios within the decades in which GMSTs were between 1.3°C and 1.7°C (1.8°C to 2.2°C) warmer than the corresponding model's reference period as a baseline.

Warming rate in each model was calculated as 1.5°C or 2°C divided by the difference between the centered timing years of each GMST rise period and the reference period (i.e., 1.5°C/2°C timing of each model in Figure 1b (or Figure S1a) minus 1880.5). Additionally, the 3°C warming rate used for analyses in Supplementary Figures was defined similarly except that GMST increase range was from 2.8°C to 3.2°C and 3°C was divided by the years GMST takes to go up 3°C from the reference period.

2.3 Low-level cloud amount feedback factor during the reference period

We used the cloud fraction at 925 hPa level as LLC amount for LLC-related analysis (see Text S1). For each model, the LLC amount feedback factor (λ_c) in the mid-latitude SO during the reference period is defined as a regression coefficient of the anomalous low-level cloud amount ($\mathrm{LLC_{MSO}}$) against the anomalous surface air temperature ($\mathrm{SAT_{MSO}}$). Here, the anomalous $\mathrm{LLC_{MSO}}$ and $\mathrm{SAT_{MSO}}$ are the areal-averaged quantities over the 30°-50°S of interannual anomalies with seasonal cycles removed from monthly LLC and SAT data.

The significance of all correlation and regression analysis performed throughout our research was tested using the bootstrap method (see Text S2).

3. Results

3.1 Near-future global warming rate and Southern Ocean state in CMIP5 climate models

First, we analyzed the years at which simulated GMSTs reached a 1.5°C/2°C increase from the pre-industrial reference period (1861-1900, hereafter referred to as 'reference period') under a business-as-usual scenario (i.e., the Representative Concentration Pathway 8.5 (RCP8.5)) in 37 CMIP5 climate model. Despite being driven by the same greenhouse gas concentrations and aerosol burdens, the results among the CMIP5 climate models were considerably diverse (Figure 1b). The BNU-ESM model reaches the 2°C limit by 2022 and shows the fastest

near-future global warming rate; the MRI-CGCM3 model simulates the slowest near-future warming rate. The number of years required to reach a 1.5°C increase is highly correlated with that for a 2°C rise (Figure 1c), and the time it takes to achieve 1.5°C and 2°C temperature rise is highly correlated with that for a 3°C increase at the 95% confidence level (Figures S2a-b). Notably, the model drift of GMST is small in each climate model compared to the 1.5°C/2°C GMST changes (Table S1), and we found that the 1.5°C/2°C timings were almost identical with and without a climate drift correction (Figures S3a-c). These results indicate that neither internal climate variability nor anthropogenic forcing is the main cause of inter-model near-future global warming rate diversity. Therefore, we propose that the systematic model states including the SO condition, cloud feedback and equilibrium climate sensitivity (ECS) are likely the reason for the large diversity among CMIP5 climate models in reaching the 1.5°C/2°C Paris Agreement limit. Hereafter, we focus on a 2°C temperature rise for near-future global warming rates in CMIP5 climate models. We note that there is little change in the results if we consider a 1.5°C temperature rise.

The ECS and/or transient climate response (TCR) are common metrics of model sensitivity in the response to increasing CO_2 (Meehl et al., 2020). ECS is defined as GMST increase until equilibrium warming following abrupt CO_2 doubling, and TCR is defined as the temperature change at the time of CO_2 doubling when CO_2 is increased by 1% yr^{-1}. The near-future warming rate of 1.5°C/2°C rise in climate models may, of course, be related to these sensitivity metrics, and can also be affected by forcing and ocean heat uptake in a complex way, making it difficult to clearly separate their roles under transient forcing (Forster et al., 2013). However, for the near future, it can be expected that the warming rate would be much more affected by physical processes occurring on shorter time scales and the related pre-warming conditions.

We found that the SO, south of 30°S, is the most critical and broad region where local warming rates highly correlate with the CMIP5 climate model 2°C global warming rate (Figure 2a). The local warming rate (Figure 2a) is calculated by dividing the local temperature increment at each grid point by the time taken from the reference period to the time when the GMST reached to 2°C in each climate model (see Text S3). While some other regions, such as the Eurasian continent, are associated with 2°C global warming rates, local SO warming rates strongly correlate with 2°C global warming rate in CMIP5 climate models. It is also found that simulated reference period SO SSTs were more highly correlated with the 2°C global warming rate simulated in CMIP5 climate models than any other ocean latitude band, including the Northern Ocean (Figure 2b and Table 1). While the correlation does not necessarily imply causality, it may indicate that the SO is a key region with the potential to regulate warming rates.

We also calculated the correlation between 2°C global warming rate and reference period SST deviation from the 37 CMIP5 climate model ensemble mean SST (Figure 2b). The reference period SO SST deviation of each climate model from the ensemble mean correlates significantly with the 2°C global warming

rate for each model. That is, the cooler is the SO SST during the reference period, the faster will be the 2°C global warming rate increase (Kajtar et al., 2021; Gjermundsen et al., 2021) (Figure 2b). Consistently, the regressed SST during the reference period against a 2°C warming rate (Figure 2c) also shows that SO SSTs during the reference period are much lower in climate models with faster warming rates than those with slow warming rates.

3.2 The role of reference period SO SST and its associated physical processes on the warming rate of 2°C temperature rise

To examine how the SO SST during the reference period is associated with the 2°C global warming rate, we first conjecture that the SO SST could be associated with ocean heat uptake, which could lead to diversity of near-future warming rates. GMST increase and decrease rates vary from model to model because of heat transfer efficiency differences (Raper et al., 2002; Winton et al., 2010; Geoffroy et al., 2013). Therefore, if the ocean heat uptake over the SO is strong, the increasing rate of GMST would be small, and vice versa. To test this notion, we calculated the change in the ocean heat content (OHC) in the SO from the reference period to the 2°C rise for each CMIP5 climate model (see Text S4) and compared the results with the SO SST and near-future warming rates. While the calculations are diverse, there is little relationship between OHC in the SO and the time it takes to achieve a temperature rise of 2°C (Figure S4a). However, the OHC in the SO is statistically more related to the years it takes to reach a 3°C temperature increase (Figure S4b), implying that the larger is the amount of heat absorbed by the SO in the time it takes to achieve a temperature increase of 3°C, the slower is the near-future warming rate. In calculating the period mean difference of OHC in the SO region (30°-70°S), the effect of the difference in ocean transport convergence is negligible (Armour et al., 2016), so the OHC can be approximated as ocean heat uptake. With the slow but persistent ocean heat uptake in the SO over the time it takes for a 3°C increase, the cumulative heat uptake seems more effective at reducing the rate of Earth's warming by trapping excess energy thereby inhibiting GMST increase. This might be related to the notion that ocean heat uptake is associated with longer-timescale deep ocean equilibration (Li et al., 2013), where the SO is the preferred location for ocean heat uptake-associated "delayed warming" (Geoffroy et al., 2013; Frölicher et al., 2015; Armour et al., 2016; Rose & Rayborn, 2016; Shi et al., 2018). These results indicate that the role of ocean heat uptake is timescale dependent. We also found that SO SST during the reference period, which is closely related to 2°C warming rate. is not related to the OHC in the SO during 2°C rise (Figure S4c). We further check the relationship between the 2ºC warming rate and the net surface heat flux changes, which allow more intuitive estimate of ocean heat uptake (e.g., Ma et al., 2020) and can directly affect SST changes, confirming that there are few or no clear correlations in the SO region (Figures S5a-b).

We hypothesize that SO SST influences the 2°C temperature increase via atmospheric radiative processes. We analyzed atmospheric heat flux changes from

the reference period to the period centered on the multi-model ensemble mean of 2°C rise timings (hereafter referred to as the MME 2°C period) (Figure 1b and see also Text S5). An increase in downward surface shortwave (SW) energy flux in the mid-latitude SO (30°-50°S) and the high-latitude SO (60°-70°S) bands is more dominant in climate models with a faster warming rate than those with a slow warming rate (Figure 3a). However, changes in the downward longwave radiation and turbulent heat fluxes including sensible heat and latent heat did not show statistically significant correlations with the 2°C warming rate (Figure 3a). Note that either + or - sign of heat flux changes in Figure 3a do not represent a heat loss or gain from the ocean to atmosphere. Indeed, the warming-related changes in the turbulent heat fluxes were identical to those presented in Liu et al. (2018) (figure not shown), that is, heat absorption through SO is mostly carried out at higher latitudes (50°S-65°S). We infer that there is a hot spot region where the SW radiative energy plays a key role in the modulation of warming (Figure 3b).

Over the mid-latitude SO, the difference in SW cloud radiative effect (SWCRE, i.e., the difference of shortwave radiative flux between clear-sky and all-sky conditions) changes is a major contributor to the difference in surface downward SW energy flux changes, whereas SWCRE has an opposite effect on incoming SW energy flux over the high-latitude SO (Figure 3b and Figure S6). We infer that the mid-latitude SW radiative energy is controlled by cloud effect, which is in contrast to the high-latitude where SW radiative energy is influenced by non-cloud components, possibly sea ice. It has been known that both LLC and Antarctic sea ice (ASI) play a prominent role in controlling the downward SW energy reaching the surface (McCoy et al., 2014; Frey et al., 2018; Loeb et al., 2019). Figures 4a and 4b display the regressed LLC and ASI concentrations during the reference period against with a 2°C warming rate. We used a 925 hPa cloud fraction to represent the LLC, since in the mid-latitude SO, the maximum cloud fraction related to 2°C warming rate is found at 925 hPa (Figure S7 and see also Text S1) and most of the observed total cloud fraction is LLC (e.g., International Satellite Cloud Climatology Project, ISCCP, Rossow & Schiffer, 1991). Climate models with fast warming rates tend to simulate relatively larger amounts of LLC in the mid-latitude SO (30°-50°S) and ASI concentrations in high-latitude SO (60°-70°S) during the reference period, compared to those with slow warming rates. The LLC amount and ASI concentration in SO region during the reference period were statistically significantly correlated with 2°C warming rate (Figures S8a-b). That is, the initially cold SO SST in fast warming rate models is interrelated with the incoming SW energy reduction caused by a large amount of LLC in the mid-latitude SO and a high reflectivity of large ASI concentration in the high-latitude SO, and vice versa for the initially warm SO SST in slow warming rate models.

And then, we calculated the LLC amount feedback factor in the mid-latitude SO (i.e., $\lambda_c = \frac{\mathrm{dLLC_{MSO}}}{\mathrm{dSAT_{MSO}}}$) during the reference period in climate models. Since λ_c is usually negative (McCoy et al., 2014; Zhao, 2014; Rose & Rayborn, 2016;

Zelinka et al., 2016; Zelinka et al., 2020), the surface cooling increases the LLC amount, resulting in further surface cooling by decreasing SW radiation (i.e., positive feedback) in the mid-latitude SO. It was found that climate models with strong LLC_{MSO} amount feedback tend to simulate a large amount of LLC_{MSO} as well as a more extended ASI with cold SO in the reference period (Figures 5a-c). We infer that LLC_{MSO} amount feedback strength determines the mid-latitude SO (30°-50°S) SST condition in the reference period by a positive shortwave-cloud feedback process. And then, the mid-latitude SST may affect the ASI (60°-70°S) through vertical oceanic warm advection by altering westerly wind strength (Armour et al., 2016; Liu et al., 2018). The higher the mid-latitude SO SST is, the stronger SST meridional gradient and consequently westerly wind are in the high-latitude SO during the reference period (Figures S9a-b). This could enhance warm advection by ocean deep convection (Armour et al., 2016; Liu et al., 2018), resulting in lower ASI concentration with also warmer SST in the high-latitude SO (Figure S9c). There might be other possibility that the larger ASI in reference state could lead to colder SO, stabilizing the atmosphere, thereby locally producing more LLC in some mid-latitude SO regions. However, as shown in Figure 4, distributions of active LLC_{MSO} and ASI for 2ºC warming rate are less overlapped, inferring that the remote effect of LLC_{MSO} on ASI might be more effective than the other way around. Therefore, here we mainly focus on a mechanism for how LLC_{MSO} amount feedback can influence ASI concentrations through coherent relationships between the climate models (figures S9a-c). During the 2ºC rise, a strong LLC_{MSO} amount feedback correlates with a large reduction of LLC_{MSO} as well as ASI (Figures 5d-e). LLC_{MSO} amount feedback will be directly linked to LLC_{MSO} changes but will rather indirectly affect ASI changes during the 2ºC rise. We speculate that LLC amount feedback can affect ASI reduction even during the 2ºC rise like in the reference period (Figures S9a-c). The ASI reduction might be affected by strong oceanic warm water convection where the zonal winds are strengthened due to the intensified SST meridional gradient in the southern high latitudes, possibly due to mid-latitude SO warming resulting from LLC_{MSO} amount feedback. The rather strong correlation in Figure 5e may be the result of a mixture of warming effects. Consequently, the reference period LLC_{MSO} amount feedback contributes significantly to determining the 2°C warming rate (Figure 5f). Here, the LLC_{MSO} amount feedback strength accounts for only 25% of the 2°C warming rate in spite of the statistical significance at the 95% confidence level (Figure 5f). This might be due to the notion that the LLC_{MSO} amount feedback influences the 2°C warming rate along with other factors including the SO SST as well as the ASI which h are affected by the LLC_{MSO} amount feedback. Nevertheless, it may not be small to explain to that extent the inter-model diversity of 2°C warming rate compared to any other single process existing in climate models.

Consistently, in the climate models simulating large amounts of mid-latitude SO LLC and high-latitude SO ASI during the reference period, the amounts of both mid-latitude SO LLC and high-latitude SO ASI tend to decrease significantly

during the 2ºC rise (Figures 6a-b). It is noteworthy that the respective variables corresponding to the reference period and the MME 2°C period in Figures 6a-b have a very high correlation with each other (Figures S10a-b). This is because the inter-model diversity of those variables still does not deviate considerably in the near-future warming period compared to that in the reference period. Therefore, the correlation coefficients shown in Figures 6a-b are not from the artificial negative initial-to-change correlations that can appear when the initial and future states are completely independent, but statistically meaningful correlations linked with physical processes. Concurrently, more downward SW energy is absorbed at the surface with a large reduction in the amount of LLC in mid-latitude SO (Figure 6c), contributing to fast global warming rates in climate models (Figure 6d). Note that more downward SW flux in mid-latitude SO comes from more SWCRE increase, which leads to faster 2ºC warming (Figures S11a-b). Additionally, more downward SW energy is absorbed at the surface with a large reduction in the ASI concentration in the high-latitude SO during the warming of 2°C temperature rise (Figure 6e) and contributes to fast global warming rates in climate models (Figure 6f). These two processes have a profound effect on the global warming rates. These results indicate that the reduction of LLC amounts and ASI concentration in the SO due to a strong LLC amount feedback could be a key factor to determine the 2°C warming rate in climate models. We argue that since the relationship between SST and cloud is not completely linear and physical environments affecting the LLC, especially an inversion layer, it would be changed under global warming. Therefore, LLC_{MSO} amount feedback may be different from the reference period to the near-future warming period. However, the stronger the LLC_{MSO} amount feedback in the reference period is (Figure S12a), the larger the change in LLC_{MSO} amount due to the same warming is and the change in LLC_{MSO} amount due to the same warming is closely related to 2°C warming rate (Figure S12b). This may imply that the LLC_{MSO} amount feedback simulated in climate models control the warming rate by driving a significant portion of the LLC_{MSO} change during the near-future warming period.

We further used the SW approximate partial radiative perturbation (APRP) method (Taylor et al., 2007) (see Text S6) to ensure how much the SWCRE change in the mid-latitude SO is driven by the LLC amount change rather than other cloud actions during the 2°C rise. We used 25 climate models in which all the variables used in APRP method are available (Table S3). It is found that cloud amount change, which is mostly explained by the LLC amount change controlling SW radiation in the mid-latitude SO regions (e.g., Rossow & Schiffer, 1991), is the most significant contributor to SW change (Table S3). Indeed, APRP estimation indicates that the SW change in the mid-latitude SO strongly correlates with LLC_{MSO} amount change during the 2°C rise as well as 2°C warming rate (Figures S13a-b). This may support the notion that the change in LLC amount along with LLC amount feedback in the mid-latitude SO contributes to modulating the 2°C warming rate by significantly controlling incoming SW radiation in climate models.

3.3 Results from CMIP6 climate models

We conducted the same analyses using 26 CMIP6 climate models with a fossil-fueled development scenario (i.e., Shared Socioeconomic Pathways (SSP) 5-8.5) and reached a similar conclusion to CMIP5 climate models. The predicted number of years required to reach a 1.5°C increase is highly correlated with that for a 2°C rise in CMIP6 climate models (Figure S1b), indicating that the systematic model state is likely the reason for the large diversity among CMIP6 climate models in reaching the 1.5°C/2°C Paris Agreement limit (Figure S1a). Like the CMIP5 climate models, the SO is a critical and broad region where local warming rates highly correlate with the 2°C global warming rate in CMIP6 climate models, but many of the correlations identified in CMIP5 climate models are rather weak in CMIP6 climate models (Figure S14a and see also Figure 2a). The most striking differences between CMIP5 and CMIP6 climate models are found in the tropical and Arctic regions. In particular, the stark opposite signal between tropics and extratropics only appears in CMIP6 climate models. This may be because the difference in the warming between the tropics and extratropics is relatively larger in CMIP6 climate models than that in CMIP5 climate models (Zelinka et al., 2020). This is possibly due to the change in the cloud scheme from CMIP5 to CMIP6 climate models, which acts to modify cloud feedback processes as well as the water content within clouds (Zelinka et al., 2020). Consequently, the sensitivity of local warming rate on the 2ºC global warming rate would be different between CMIP5 and CMIP6 climate models.

We also found that, similar to the CMIP5 climate models, simulated reference period SO SSTs were more highly correlated with the 2°C global warming rate simulated in CMIP6 climate models than with any other ocean latitude band, including the Northern Ocean (Table S2 and Figure S14b and see also Figure 2b). That is, SO SSTs during the reference period are much cooler in climate models with faster warming rates than those with slow warming rates in CMIP6 climate models. In addition, the CMIP6 climate models with fast warming rates tend to produce larger amounts of LLC in mid-latitude SO and higher ASI concentrations in high-latitude SO compared to those with slow warming rates (Figures S15a-b), implying that the 2°C warming rate simulated in CMIP6 climate models is statistically significantly correlated with the LLC amount, and the ASI extent during the reference period.

Consistent with CMIP5 climate models, CMIP6 climate models with a strong LLC_{MSO} amount feedback also tend to simulate a large amount of LLC_{MSO} in the reference period (Figure S16a), which is concurrent with a cold SO (Figure S16b). During the 2°C rise, the amount of LLC_{MSO} is more reduced in CMIP6 climate models (Figure S16c) along with more increases in downward SW energy flux and SWCRE (Figures S16d-e), which is due to stronger LLC_{MSO} amount feedback. This results in a fast-warming rate (Figure S16f), which is consistent with the results in CMIP5 climate models.

4. Conclusions and Discussion

The SO is a critically important global climate system sector (e.g., Sabine et al., 2004; Brady, 2011; Kuhlbrodt & Gregory, 2012; Roemmich et al., 2015). Despite this, there are many deficiencies in correctly representing the SO in climate models (Sallée et al., 2013; Meijers, 2014; Hyder et al., 2018). Our research emphasizes the importance of realistic SO simulations during the reference period including SST, ASI, LLC, and LLC amount feedback in CMIP5/CMIP6 climate models to reduce the uncertainty of the near-future global warming rate. As the temperatures rise to the 2°C increase, their changes alter the amount of downward SW energy flux at the surface and affect the warming rates.

On the other hand, Gjermundsen et al. (2021) argued that the rate of SO warming influences the effective climate sensitivity and the global warming rate via SO cloud feedbacks. They emphasized that climate models with warmer SO SSTs than normal in the pre-industrial state, which is due to vigorous deep ocean convection, show less SO warming under greenhouse forcing as convection shuts down. This leads to delayed emergence of positive SW cloud feedback, resulting in less global warming. The pre-industrial SO conditions could be affected not only by LLC amount feedback but also by SO deep convection. However, the acting time scales of cloud feedback and deep ocean circulation may be different in transient climate simulations. Therefore, LLC amount feedback can be more important in the near-future warming, even if the role of deep ocean circulation may become more important in the longer-future warming. This is also supported by the fact that OHC in the SO is significantly correlated to 3°C warming rate but not to 2°C warming rate (Figures S4a-b) as well as the relationship of the intensity of southern meridional overturning circulation (Gjermundsen et al., 2021) in the reference period with 2°C and 3°C warming rates in CMIP5 and CMIP6 climate models, respectively (Figures S17a-d). Although SW cloud feedback and deep-ocean warming are not completely independent in SO, controlling the amount of incoming SW through fast-paced cloud feedback could be more important for near-future warming rate in climate models.

Since only one ensemble member was used and the reference period was defined as a period of 40 years in our analysis, the climatology in this period might be influenced by the phase of interdecadal variability. However, as shown in Figures 2c-b, dominant interdecadal patterns such as Atlantic Multidecadal Oscillation, Pacific Decadal Oscillation, and Interdecadal Pacific Oscillation, which would be expected if they importantly affect near-future warming, were not shown. From this, we could identify that the inter-model diversity of SO condition in the reference period related to near-future warming rate is hardly derived from the phase dependency of interdecadal variability. In addition, spin-up, an important technical issue of the coupled model, is also a factor that can affect the climate state represented in each model. Nevertheless, our findings physically consistently account for a large part of inter-model diversity in near-future warming. Therefore, we argue that the SO condition in the reference period can largely represent the model dependency, which may imply both physical aspects and technical aspects in each model. Although there might be differences between climate models in the used parameterization/scheme or bias of

the atmospheric model affecting the implementation of this feedback in SO region (e.g., Hyder et al., 2018), the physical aspects are highlighted in the present study. We point out that LLC amount feedback influences the SO condition of model climatology in the reference period, and furthermore a 2°C near-future global warming rate is effectively determined by the SO condition with an LLC amount feedback strength during the reference period. Our results suggest that accurate simulation of the pre-industrial SO state with LLC amount feedback will serve as a critical factor in future target warming climate projections.

Data Availability Statement

All data used in this study are publicly available. HadCRUT4 is available at https://www.metoffice.gov.uk/hadobs/hadcrut4/data/current/download.html. CMIP5 data provided by ESGF can be obtained from the open-source link: https://esgf-index1.ceda.ac.uk/search/cmip5-ceda/. Users should select Frequency as *monthly*, Experiment ID as *historical or rcp85*, Ensemble as *r1i1p1*, Model as CMIP5 models used for analyses in this study, and then download the nc files of the required variables by opening them one by one from the list that appears as search outputs. For CMIP6 data, the open-source link is https://esgf-node.llnl.gov/search/cmip6/. It is the same as the case of obtaining CMIP5 data, but Experiment ID is *historical or ssp585* and Variant Label is *r1i1p1f1*. The codes used in this study for Bootstrap and APRP calculation can be accessed at https://www.ncl.ucar.edu/Applications/bootstrap.shtml and https://github.com/mzelinka/aprp/blob/master/code/python/demonstrate_APRP.py, respectively.

Acknowledgments

No known conflicts of interest of the authors exist. This work was supported directly by National Research Foundation of Korea (NRF-2018R1A5A1024958), Yonsei Signature Research Cluster Program of 2021 (2021-22-0003).

References

1. Armour, K., Marshall, J., & Scott, J., et al. (2016). Southern Ocean warming delayed by circumpolar upwelling and equatorward transport. *Nature Geoscience*, *9*, 549–554.

2. Baker, H. S., et al. (2018). Higher CO_2 concentrations increase extreme event risk in a 1.5°C world. *Nature Climate Change*, *8*, 604–608.

3. Bony, S., & Dufresne, J. L. (2005). Marine boundary layer clouds at the heart of tropical cloud feedback uncertainties in climate models. *Geophysical Research Letters*, *32*, 1–4.

4. Brady, A. M. (2011). Science Diplomacy: Antarctica, Science, and the Governance of International Spaces. 301–302.

5. Briffa, K. R., Van der Schrier, G. & Jones, P. D. (2009). Wet and dry summers in Europe since 1750: evidence of increasing drought. *International Journal of Climatology*, *29*, 1894–1905.

6. Brown, S., et al. (2018). Quantifying Land and People Exposed to Sea-Level Rise with No Mitigation and 1.5°C and 2.0°C Rise in Global Temperatures to Year 2300. *Earth's Future*, *6*, 583–600.

7. Cess, R. D., et al. (1990). Intercomparison and interpretation of climate feedback processes in 19 atmospheric general circulation models. *Journal of Geophysical Research: Atmospheres*, *95*(D10), 16601-16615.

8. Christidis, N., Stott, P. A., & Brown, S. J. (2011). The role of human activity in the recent warming of extremely warm daytime temperatures. *Journal of Climate*, *24*, 1922-1930.

9. Dai, A. (2011). Drought under global warming: a review. *WIREs Climate Change*, *2*, 45-65.

10. Dommenget, D. (2016). A simple model perturbed physics study of the simulated climate sensitivity uncertainty and its relation to control climate biases. *Climate Dynamics*, *46*, 427–447.

11. Donnelly, C., et al. (2017). Impacts of climate change on European hydrology at 1.5, 2 and 3 degrees mean global warming above preindustrial level. *Climatic Change*, *143*, 13–26.

12. Duffy, P. B., & Tebaldi, C. (2012). Increasing prevalence of extreme summer temperatures in the U.S. *Climatic Change, 111*, 487-495.

13. Ebi, K. L., et al. (2018). Health risks of warming of 1.5°C, 2°C, and higher, above pre-industrial temperatures. *Environmental Research. Letters*, *13*, 063007.

14. Forster, P. M., Andrews, T., Good, P., Gregory, J. M., Jackson, L. S., & Zelinka, M. (2013). Evaluating adjusted forcing and model spread for historical and future scenarios in the CMIP5 generation of climate models, *Journal of Geophysical Research: Atmospheres*, *118*, 1139– 1150.

15. Frey, W. R., Morrison, A. L., Kay, J. E., Guzman, R., & Chepfer, H. (2018). The Combined Influence of Observed Southern Ocean Clouds and Sea Ice on Top-of-Atmosphere Albedo. *Journal of Geophysical Research: Atmosphere*, *123*, 4461–4475.

16. Frölicher, T. L., et al. (2015). Dominance of the Southern Ocean in anthropogenic carbon and heat uptake in CMIP5 models. *Journal of Climate*, *28*, 862–886.

17. Frölicher, T. L., Winton, M., & Sarmiento, J. L. (2014). Continued global warming after CO_2 emissions stoppage. *Nature Climate Change*, *4*, 40–44.

18. Geoffroy, O., et al. (2013). Transient climate response in a two-layer energy-balance model. Part II: Representation of the efficacy of deep-ocean heat uptake and validation for CMIP5 AOGCMs. *Journal of Climate*, *26*, 1859–1876.

19. Gjermundsen, A., Nummelin, A., & Olivié, D., et al. (2021). Shutdown of Southern Ocean convection controls long-future greenhouse gas-induced warming. *Nature Geoscience*, *14*, 724–731.

20. Hyder, P., et al. (2018). Critical Southern Ocean climate model biases traced to atmospheric model cloud errors. *Nature Communication*, *9*.

21. Kajtar, J. B., Santoso, A., Collins, M., Taschetto, A. S., England, M. H., & Frankcombe, L. M. (2021). CMIP5 Intermodel Relationships in the Baseline Southern Ocean Climate System and With Future Projections. *Earth's Future*, *9*, e2020EF001873.

22. Knutti, R., Masson, D., & Gettelman, A. (2013). Climate model genealogy: Generation CMIP5 and how we got there. G*eophysical Research Letters*, *40*, 1194–1199.

23. Knutti, R., Rugenstein, M. A. A., & Hegerl, G. C. (2017). Beyond equilibrium climate sensitivity. *Nature Geoscience*, *10*, 727–736.

24. Kuhlbrodt, T., & Gregory, J. M. (2012). Ocean heat uptake and its consequences for the magnitude of sea level rise and climate change. *Geophysical Research Letters*, *39*(18).

25. Li, C., Von Storch, J. S., & Marotzke, J. (2013). Deep-ocean heat uptake and equilibrium climate response. *Climate Dynamics*, *40*, 1071–1086.

26. Liu, W., Lu, J., Xie, S., & Fedorov, A. Southern Ocean Heat Uptake, Redistribution, and Storage in a Warming Climate: The Role of Meridional Overturning Circulation. *Journal of Climate*, *31*, 4727-4743.

27. Loeb, N. G., et al. (2019). Decomposing shortwave top-of-atmosphere and surface radiative flux variations in terms of surface and atmospheric contributions. *Journal of Climate*, *32*, 5003–5019.

28. Masson-Delmotte, V., et al. (2018). Global warming of 1.5 °C. In An IPCC Special Report on the impacts of global warming of 1.5 °C above pre-industrial levels and related global greenhouse gas emission pathways, in the context of strengthening the global response to the threat of climate change, sustainable development, and efforts to eradicate poverty. *In Press* 2018.

29. Masson-Delmotte, V., et al. (2021). Climate Change 2021: The Physical Science Basis. Contribution of Working Group I to the Sixth Assessment Report of the Intergovernmental Panel on Climate Change. *Cambridge University Press. In Press* 2021.

30. Ma, X., Liu, W., Allen, R. J., Huang, G., & Li, X. (2020). Dependence of regional ocean heat uptake on anthropogenic warming scenarios. Science advances, 6, eabc0303.

31. McCoy, D. T., Hartmann, D. L., & Grosvenor, D. P. (2014). Observed Southern Ocean cloud properties and shortwave reflection. Part I: Calculation of SW flux from observed cloud properties. *Journal of Climate*, *27*, 8836–8857.

32. Meehl, G. A., Senior, C. A., Eyring, V., Flato, G., Lamarque, J. F., Stouffer, R. J., Taylor, K. E., & Schlund, M. (2020). Context for interpreting equilibrium climate sensitivity and transient climate response from the CMIP6 Earth system models. *Science Advances*, *6*(26), eaba1981.

33. Meijers, A. J. S. (2014). The Southern Ocean in the coupled model intercomparison project phase 5. *Philosophical Transactions of the Royal Society A: Mathematical, Physical and Engineering Sciences*, *372*(2019), 20130296.

34. Mitchell, J. M., et al. (1966). Climatic changes. *WMO Technical. Note 79*, *WMO 195*, 81.

35. Morice, C. P., Kennedy, J. J., Rayner, N. A., & Jones, P. D. (2012). Quantifying uncertainties in global and regional temperature change using an ensemble of observational estimates: The HadCRUT4 dataset, *Journal of Geophysical Research*, *117*, D08101.

36. Niederdrenk, A. L., & Notz, D. (2018). Arctic Sea Ice in a 1.5°C Warmer World. *Geophysical Research Letters*, ***45***, 1963–1971.

37. Raper, S. C. B., Gregory, J. M., & Stouffer, R. J. (2002). The role of climate sensitivity and ocean heat uptake on AOGCM transient temperature response. *Journal of Climate*, *15*, 124–130.

38. Roemmich, D., et al. (2015). Unabated planetary warming and its ocean structure since 2006. *Nature Climate Change*, *5*, 240–245.

39. Rose, B. E. J., & Rayborn, L. (2016). The Effects of Ocean Heat Uptake on Transient Climate Sensitivity. *Current Climate Change Reports*, *2*, 190–201.

40. Rossow, W. B., & Schiffer, R. A. (1991). ISCCP cloud data productions. *Bulletin of the American Meteorological Society*, *72*, 2-20.

41. Sabine, C. L., et al. (2004). The oceanic sink for anthropogenic CO_2. *Science*, *305*, 367–371.

42. Sallée, J. B., et al. (2013). Assessment of Southern Ocean water mass circulation and characteristics in CMIP5 models: Historical bias and forcing response. *Journal of Geophysical Research: Oceans*, *118*, 1830–1844.

43. Scheffer, M., Brovkin, V., & Cox, P. M. (2006). Positive feedback between global warming and atmospheric CO_2 concentration inferred from past climate change. *Geophysical Research Letters*, *33*, L10702.

44. Shi, J. R., Xie, S. P., & Talley, L. D. (2018). Evolving relative importance of the Southern Ocean and North Atlantic in anthropogenic ocean heat uptake. *Journal of Climate*, *31*, 7459–7479.

45. Smith, P., Price, J., Molotoks, A., Warren, R., & Malhi, Y. (2018). Impacts on terrestrial biodiversity of moving from a 2°C to a 1.5°C target. *Philosophical Transactions: Mathematical, Physical and Engineering Sciences*, *376*, 20160456.

46. Soden, B. J., & Held, I. M. (2006). An assessment of climate feedbacks in coupled ocean-atmosphere models. *Journal of Climate*, *19*, 3354–3360.

47. Taylor, K. E., Crucifix, M., Braconnot, P., Hewitt, C. D., Doutriaux, C., Broccoli, A. J., Mitchell, J. F. B., & Webb, M. J. (2007). Estimating shortwave radiative forcing and response in climate models. *Journal of Climate*, 20, 2530-2543.

48. Winton, M., Takahashi, K., & Held, I. M. (2010). Importance of Ocean Heat Uptake Efficacy to Transient Climate Change. *Journal of Climate*, *23*, 2333–2344.

49. Zelinka, M. D., et al. (2020). Causes of Higher Climate Sensitivity in CMIP6 Models. *Geophysical Research. Letters*, *47*(1), e2019GL085782.

50. Zelinka, M.D., Zhou, C., & Klein, S. A. (2016). Insights from a refined decomposition of cloud feedbacks. *Geophysical Research Letters*, *43*, 9259–9269.

51. Zhao, M. (2014). An investigation of the connections among convection, clouds, and climate sensitivity in a global climate model. *Journal of Climate*, *27*, 1845–1862.

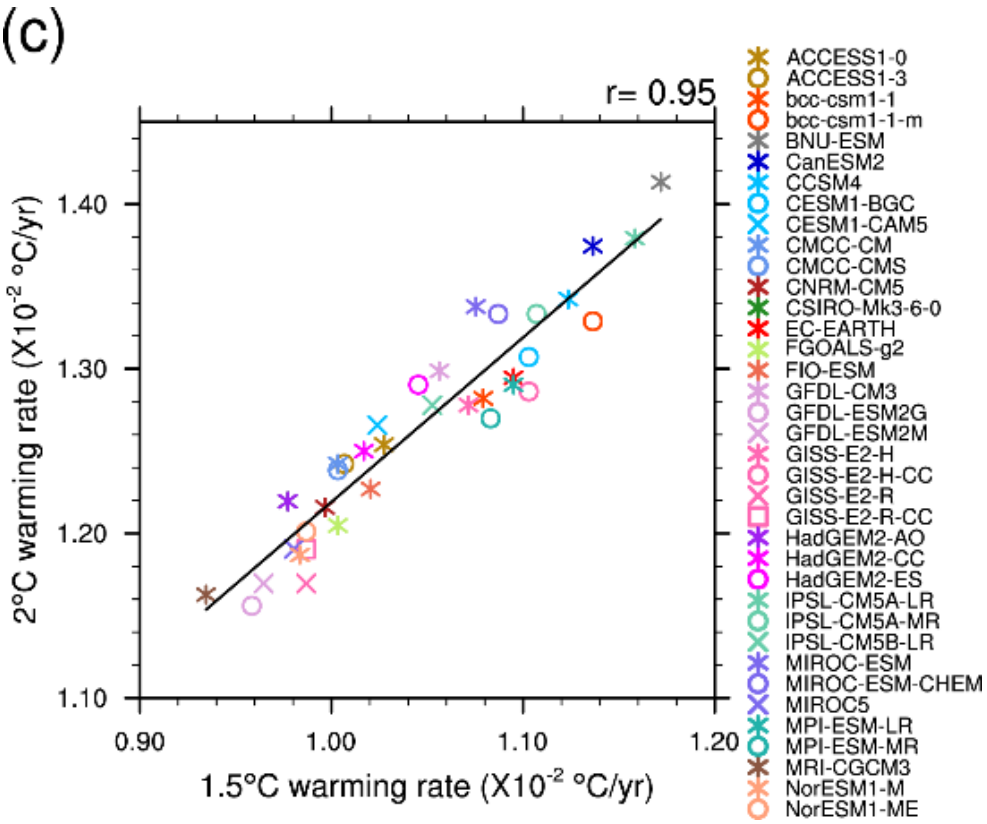

Figure 1. Observed GMST and simulated timings and global warming rates of 1.5℃/2℃ increases. (a) Observed annual anomalies of GMST relative to the reference period (1861-1900). (b) Orange and red dots indicate timings when the global mean surface temperature increases by 1.5℃ and 2℃, respectively, compared to the reference period for 37 CMIP5 climate models. MME mean values of the timings are also shown at the rightmost. (c) Linear relationship between global warming rates of 1.5℃ and 2℃. Correlation coefficient between the two rates is 0.95, which is significant at the 95% confidence level under the Bootstrap method.

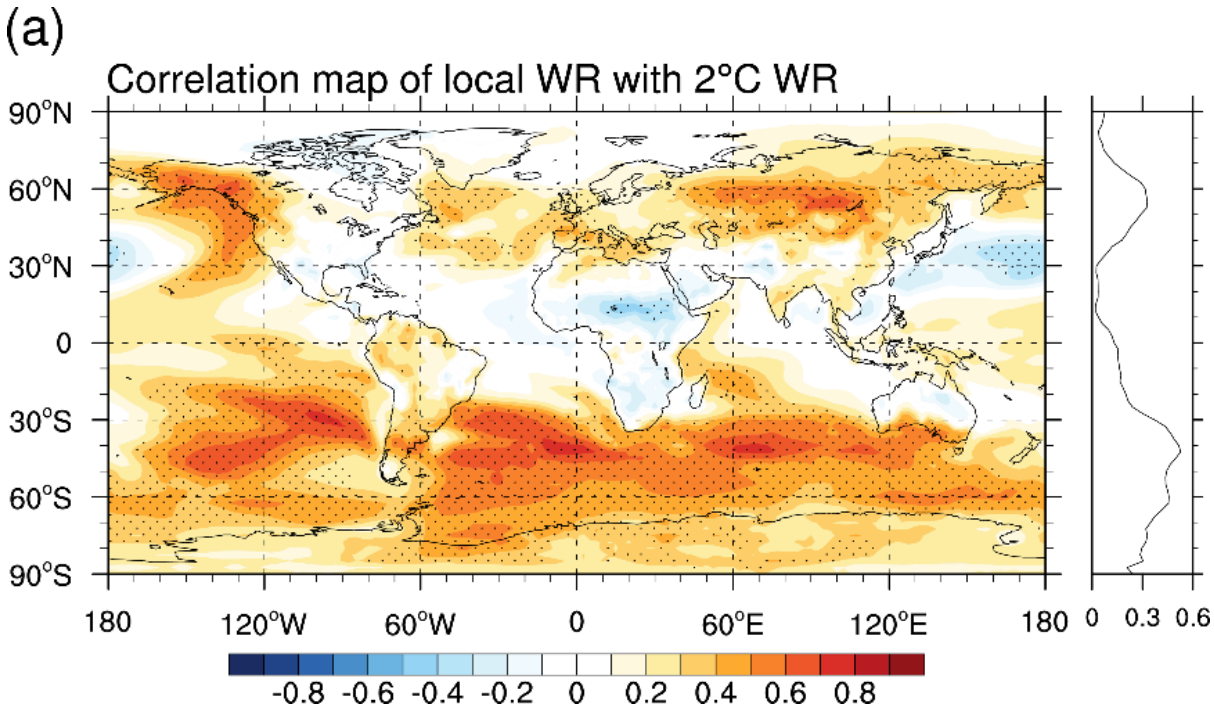

Figure 2. Southern Ocean surface related to the 2°C warming rate. (a) Correlation coefficient map of local warming rate patterns with 37 CMIP5 climate model global warming rates until a 2°C GMST increase is reached. Zonal mean is attached to the right side of the plot. (b) Correlation coefficient map of the deviation pattern from the MME mean for the SST reference period and the 2°C warming rate. (c) Map of the reference period SST regressed onto the 2°C warming rate. The stippled areas indicate regions with significant correlation or regression coefficient values at the 95% confidence level under the Bootstrap method.

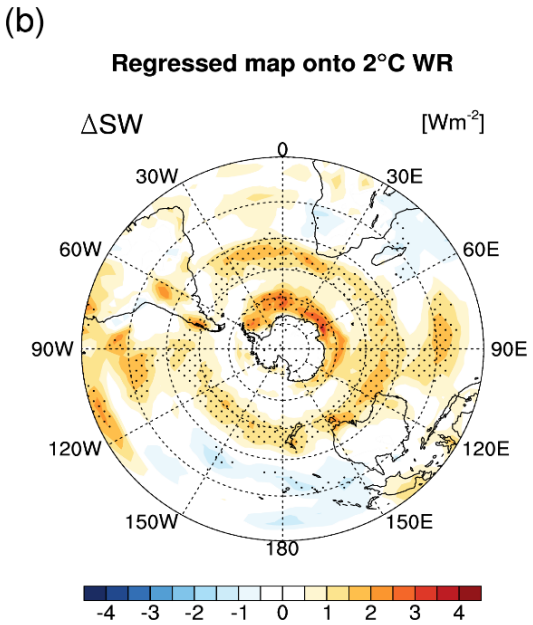

Figure 3. Southern Ocean SW flux changes associated with the 2°C warming rate. (a) Zonal mean changes from the reference period to the MME 2°C period in surface SW radiation, longwave radiation, and turbulent (sensible and latent) heat fluxes regressed onto the 2°C warming rate. The open circles denote significant differences at the 95% confidence level under the Bootstrap method. There are no significant relations to the 2°C warming rate for LW and SH+LH fluxes. (b) Map of surface SW flux changes regressed onto the 2°C warming rate. The stippled areas indicate regions with significant regression coefficient values at the 95% confidence level under the Bootstrap method. Positive values mean greater fluxes enter the surface. Images are only shown for the southern hemisphere.

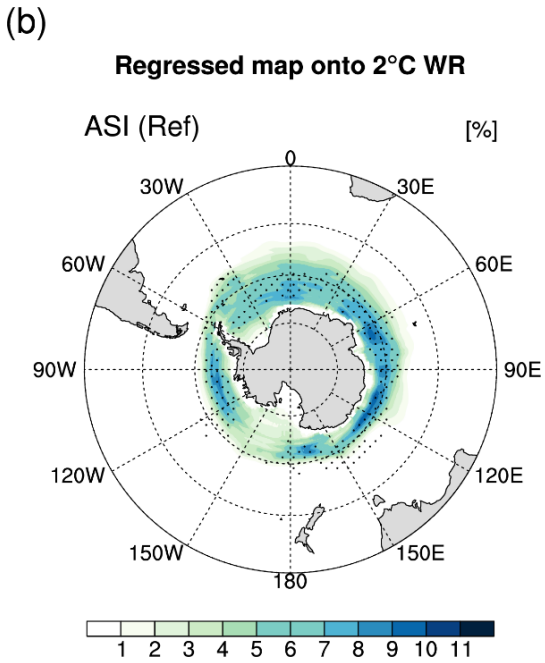

Figure 4. Reference period Low-level cloud (LLC) and Antarctic sea-ice (ASI) changes related to the 2°C warming rate through their changes. Maps of the reference period showing (a) LLC amount, characterized by LLC fraction at 925hPa and (b) ASI concentration regressed onto the 2°C warming rate. The stippled areas indicate regions with significant regression coefficient values at the 95% confidence level under the Bootstrap method. Images show the region south of 30°S.

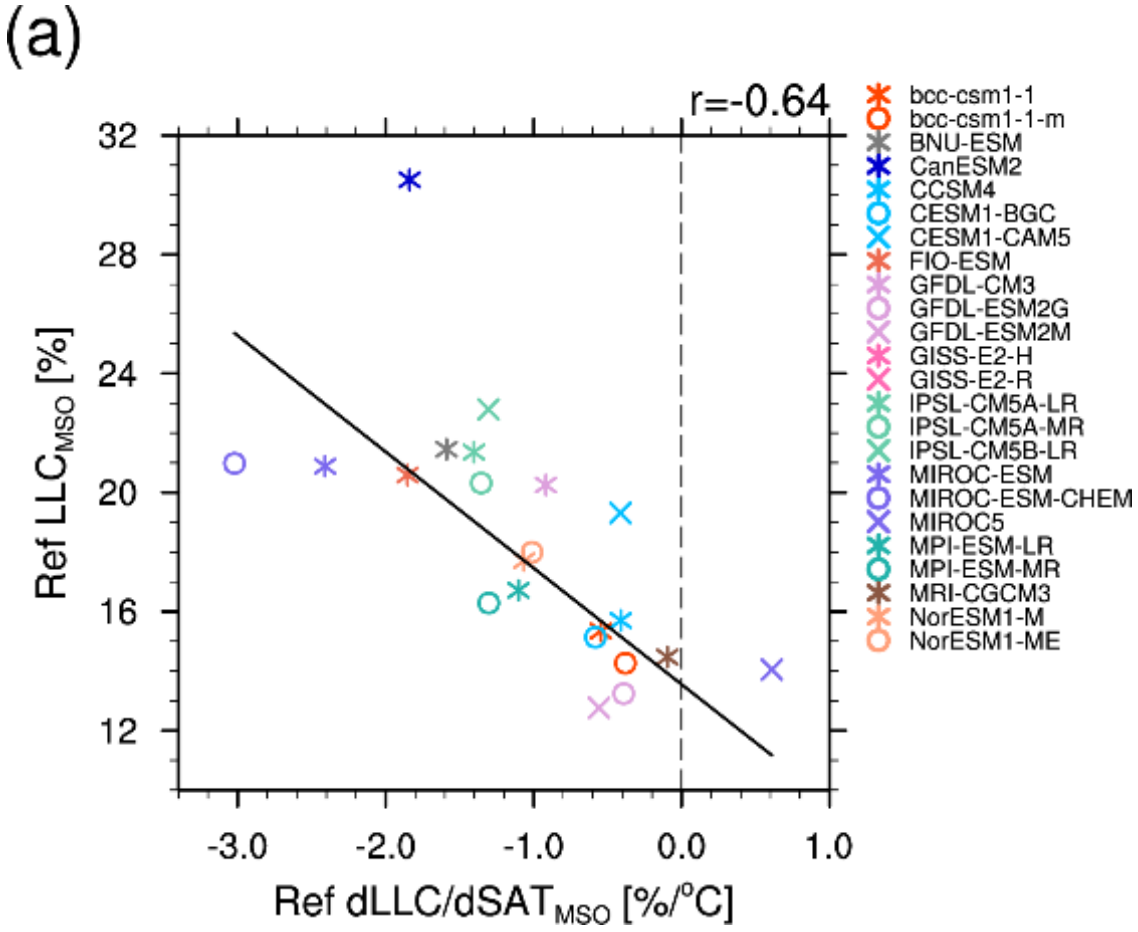

Figure 5. Low-level cloud (LLC) amount feedback and its relevant quantities. (a) Scatter plot symbols show the relationship between LLC amount (i.e., 925hPa cloud fraction) feedback factor during the reference period and the reference period LLC amount in the mid-latitude SO (30°-50°S) among the 24 CMIP5 climate models from which we can get LLC amount data. Same as (a), except for (b) the reference period ASI extent, (c) the reference period SO (30°-70°S) SST, (d) LLC amount changes in the mid-latitude SO (30°-50°S) from the reference period to the MME 2°C period, (e) ASI extent changes from the reference period to the MME 2°C period, and (f) the 2°C warming rate. The correlation coefficient between the x-axis and the y-axis variables is shown in the upper right corner of each panel, significant at the 95% confidence level under the Bootstrap method.

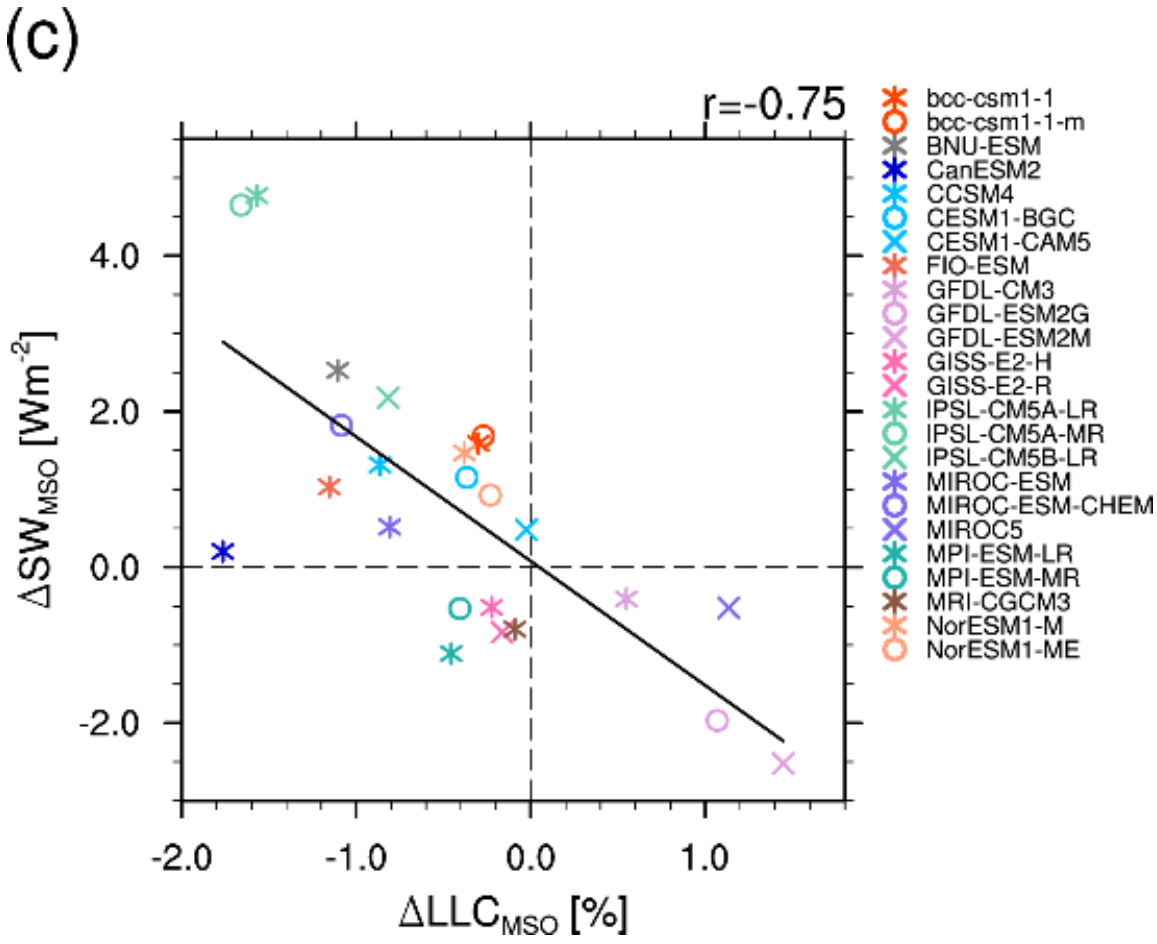

Figure 6. Impacts of Low-level cloud (LLC) and Antarctic sea-ice (ASI) through SW flux changes at a 2°C warming rate. (a) Scatter plot symbols showing the relationship between the reference period LLC amount (i.e., 925hPa cloud fraction) and its changes from the reference period to the MME 2°C period in the mid-latitude SO (30°-50°S) among the 24 CMIP5 climate models. (b) Scatter plot symbols showing the relationship between the reference period ASI extent and its changes from the reference period to the MME 2°C period among the 37 CMIP5 climate models. (c) Scatter plot symbols show the relationship between LLC amount changes and surface SW flux changes from the reference period to the MME 2°C period in the mid-latitude SO (30°-50°S) among the 24 CMIP5 climate models. (d) Scatter plot symbols show the relationship between surface SW flux changes in the mid-latitude SO and 2°C warming rate among the 35 CMIP5 climate models from which net surface SW flux data is available. (e) Scatter plot symbols show the relationship between ASI extent changes and surface SW flux changes in the high-latitude SO (60°-70°S) among the 35 CMIP5 climate models. (f) Scatter plot symbols show the relationship

between surface SW flux changes in the high-latitude SO and the 2°C warming rate among the 35 CMIP5 climate models. The correlation coefficient between the x-axis and the y-axis variables is shown in the upper right corner of each panel, significant at the 95% confidence level under the Bootstrap method.

Table 1. Relative regional mean SST during reference period to the global warming rate. Correlation coefficients with a 1.5°C/2°C warming rate of regional mean (30°S-70°S, 30°S-30°N, and 30°N-70°N) SSTs during the reference period from the 37 CMIP5 climate models. Only the correlation coefficients with SSTs in the Southern Ocean region are significant at the 95% confidence level under the Bootstrap method.

	Regional mean SST during reference period		
	°-70°S (Southern Ocean)	°S-30°N (Tropical ocean)	°-70°N (Northern ocean)
°C warming rate			
°C warming rate			